ANNALS OF GEOPHYSICS, 69, 2026; doi:10.4401/ag-9604
OPEN ACCESS

Database of HVSR Measurements Across the Mt. Etna (Sicily, Italy)

Iolanda Gaudiosi[1], Carla Barnaba[*,2], Giovanna Laurenzano[2], Francesco Pennica[1], Maurizio Simionato[1], Raffaele Azzaro[3], Graziano Boniolo[1], Giulio Brunelli[3], Stefano Catalano[4], Giuseppe Cavuoto[5], Federica Davani[1,7], Vincenzo di Fiore[5], Daniela Famiani[3], Sabrina Grassi[4], Salomon Hailemikael[3], Sebastiano Imposa[4], Marco Mancini[1], Giuliano Milana[3], Gabriele Morreale[4], Daniela Niceforo[6], Francesco Panzera[4], Mario Paratore[3], Edoardo Peronace[1], Claudia Pirrotta[4], Attilio Porchia[1], Michele Punzo[5], Luca Maria Puzzilli[6], Gabriele Quattrocchi[4], Marco Romanelli[2], Valerio Ruscito[6], Daniela Tarallo[5], Perla Taverna[9], Antonio Torrisi[8], Giuseppe Tortorici[1], Giuseppina Tusa[3], Roberto de Franco[1], Grazia Maria Caielli[1]

(1) Istituto di Geoscience (formerly Istituto di Geologia Ambientale e Geoingegneria), Consiglio Nazionale delle Ricerche, Italy
(2) Istituto Nazionale di Oceanografia e di Geofisica Sperimentale, Italy
(3) Istituto Nazionale di Geofisica e Vulcanologia, Italy
(4) Università di Catania, Dipartimento di Scienze Biologiche, Geologiche e Ambientali (DBGES), Catania, Italy
(5) Istituto di Scienze del Patrimonio Culturale, Consiglio Nazionale delle Ricerche, Italy
(6) Istituto Superiore per la Protezione e la Ricerca Ambientale, Rome, Italy
(7) Università di Trieste, Dipartimento di Matematica, Informatica e Geoscienze, Trieste, Italy
(8) Dipartimento Regionale Protezione Civile della Presidenza della Regione Siciliana, Nicolosi (CT), Italy
(9) Università di Ferrara, Dipartimento di Fisica e Scienze della Terra, Italy

Article history: received April 30, 2026; accepted August, 3, 2026

Abstract

The Mt. Etna is characterized by complex geological, volcanic and seismological dynamics, making geophysical site characterization particularly challenging.

This work presents a harmonized database of Horizontal-to-Vertical Spectral Ratio (HVSR) measurements acquired across multiple municipalities in the Etna area, including both urban and rural sites. The dataset integrates field surveys conducted by different teams using standardized acquisition and processing procedures.

All recordings were validated through HVSR consistency checks, metadata verification, and cross-comparison among different instruments.

The database provides a valuable resource for seismic microzonation, site-response numerical modelling, and multidisciplinary studies on the Mt. Etna region. It is intended to support both ongoing research and future investigations by the scientific community.

Keywords: geophysical dataset; ambient vibration; HVSR; Etna region; spectral analysis

1. Introduction

Ambient noise is widely recognized as a very powerful tool to retrieve the resonance frequency of soil deposits, according to the horizontal-to-vertical-spectral-ratio (HVSR). This is particularly important in urban areas, for evaluating possible interactions with the building's resonance (Gallipoli et al., 2004).

Moreover, ambient noise measurements are important for the identification of depths of the main impedance contrasts within the soil column, generally corresponding to the interface between soft soil material and the stiff bedrock (D'Amico et al., 2008; Mascandola et al., 2019; Parolai et al., 2019).

In this perspective, this paper reports and examines part of the geophysical measurements collected within an interinstitutional project called "ETNA-FAC-MS" which involves the Civil Protection Department of the Sicily Region, several Italian Public Research Institutions and Universities belonging to the Center for Seismic Microzonation and its applications (hereinafter CentroMS, https://centromicrozonazionesismica.it/en).

The main aim of "ETNA-FAC-MS" project is the identification, classification and characterization (type, dimension of the fault susceptibility zones and related uncertainty) of the Active and Capable Faults (FAC) of the Mount Etna Volcano (Sicily), which differ from the active faults controlled exclusively by regional tectonics (Technical Commission on Seismic Microzonation, 2015; Peronace et al., 2026).

Nevertheless, within the same project, several complementary activities were carried out, including the empirical estimation of site amplification factors (Laurenzano et al., this issue) and new geognostic and geophysical acquisitions (Porchia et al., 2026). The latter served two distinct purposes: on the one hand, to investigate new indicators potentially associated with the presence of faults; on the other hand, to expand the dataset of available measurements for seismic microzonation purposes.

This work is not a unique experiment in the Italian scientific panorama: during the 2016-2017 seismic sequence of Central Italy, CentroMS supported the largest and most complex study of post-event seismic microzonation in Italy (Imposa et al., 2017; Moscatelli et al., 2020). In that case, similar data, including seismic recordings acquired during the seismic emergencies phase, were employed in microzonation studies to evaluate site response functions, amplification factors, response spectra, and as benchmark for numerical simulations (Cara et al., 2018).

Worldwide, another example of an HVSR database is the one of strong motion stations mainly located in California, made publicly available as an additional feature of the shear wave velocity profile database (Gospe et al., 2022; Wang et al., 2022, 2023). Also records from Centre Port along with other data characterizing the subsurface of Wellington, New Zealand, were assembled and publicly available through the Design Safe-CI under the title 'Dynamic Characterization of Wellington, New Zealand' (Cox and Vantassel, 2018). All database shares the same model of many literature works (i.e., the site characterization database of the Swiss Seismological Service, Hobiger et al., 2021; the CRISP database, Cultrera et al., 2022).

The archive of HVSR of this study, organized in an interoperable format, can be used to:

- improve the detection of the resonance frequencies by comparing the sensitivity of different instrumentations;
- test the consistency of HVSR derived from different data sources, in particular by comparing microtremors from permanent stations and temporary arrays acquired at the same site;
- find and test best practices for HVSR data acquisition and processing.

After a brief description of the geological and seismological setting of the study area, we will present the data sources, signal processing, and analysis procedures used to compute HVSR. We will also describe routines to evaluate the presence of peaks and to identify HVSR-related parameters relevant for site response studies.

In the conclusions we summarize the scope and principal findings of this study and recommendation for future work to facilitate the use of HVSR for seismic risk mitigation in the Etnean area.

2. Geological-Structural and Seismotectonic Setting with Observed Ground Effects

Mt. Etna is one of the most active volcanoes in the world, rising to an elevation of approximately 3350 m, and it is characterized by several active volcano-tectonic lineaments mainly located in the eastern and southern sectors of the volcano (Fig. 1), which is subject to gravitational collapse toward the Ionian Sea (Azzaro et al., 2012). The fault systems in the area exhibit normal, strike-slip, and oblique-slip kinematics, as inferred from surface faulting features and focal mechanisms (Azzaro, 1999; Catalano et al., 2013). Earthquakes are very shallow (hypocenters mostly within 2 km depth) and produce surface fracturing and deformation around the recognized emerging fault zones even for moderate magnitude events (Mw > 4), causing widespread damage to buildings. The main onshore faults are: TMF: Tremestieri; TCF: Trecastagni; ACRF: Acireale; FF: Fiandaca; STF: Santa Tecla; PF: Pernicana (Fig. 1). The Mw 4.9 earthquake of 26 December 2018 reactivated the Fiandaca Fault, producing a coseismic ground-fracture field located several hundred meters northeast of the surface rupture zones mapped after historical earthquakes. The active Pernicana fault system (PF) represents the most significant tectonic structure in the study area.

Several previous studies have examined seismic site response at Mt. Etna, mainly using ambient noise measurements and HVSR technique. These investigations revealed the highly heterogeneous behaviour of the volcanic edifice, with strong lateral variations in site amplification related to the complex alternation of lava flows, volcaniclastic deposits, and structural discontinuities, and highlighted directional variations of resonance (Di Giulio et al., 2009; Imposa et al., 2004; Panzera et al., 2016, 2017; Pischiutta et al., 2013).

Furthermore, a systematic polarization of ambient noise, near perpendicular to the main faults, was found along several Mt. Etna faults – including Moscarello, Aci Catena, Tremestieri, and Pernicana – in previous studies (Rigano et al., 2008).

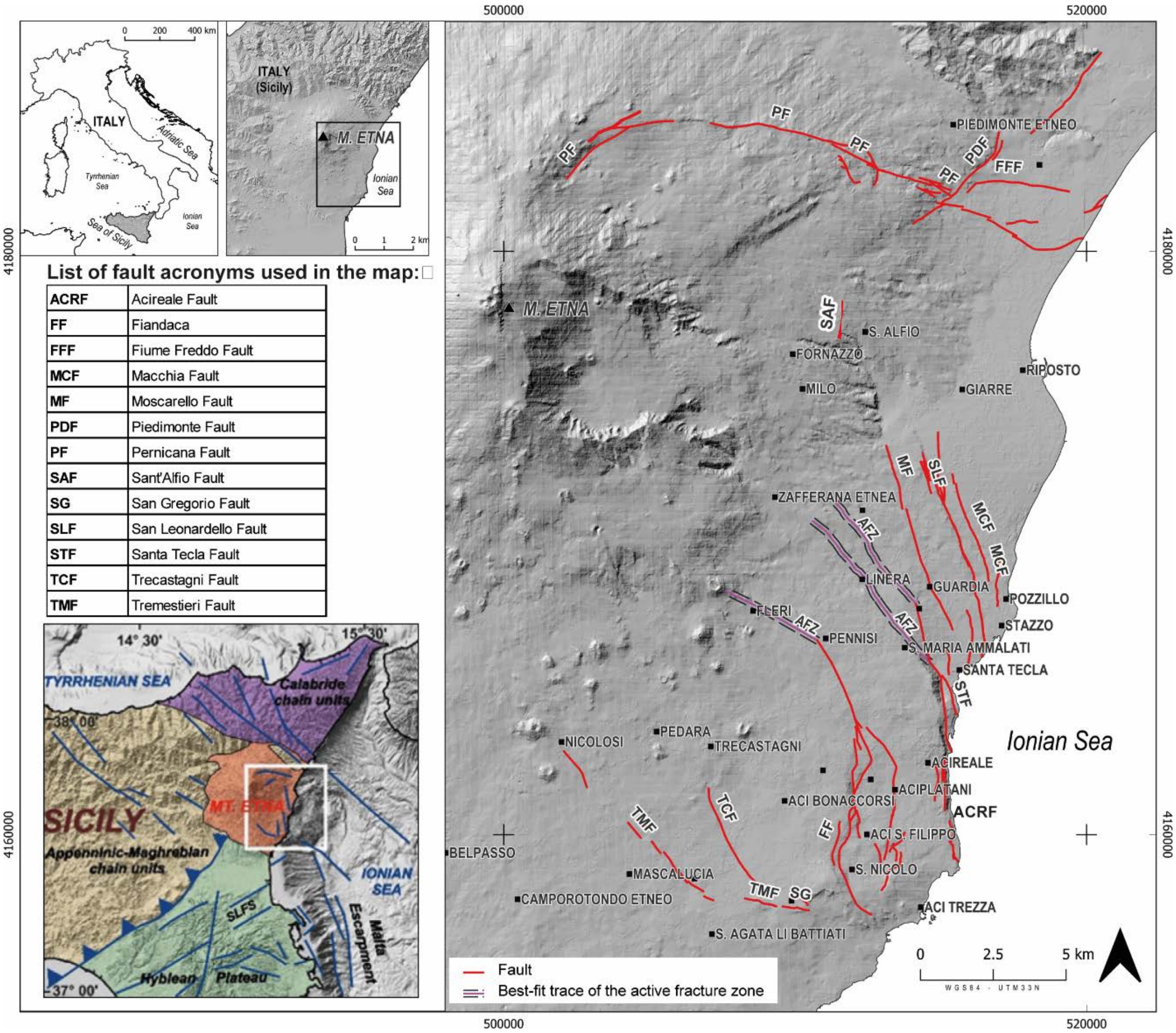

Figure 1. Volcano-tectonic map of the eastern flank of Mt. Etna volcano from Azzaro et al. (2012); main onshore faults: TMF: Tremestieri; TCF: Trecastagni; ACRF: Acireale; FF: Fiandaca; STF: S. Tecla; PF: Pernicana. The inset displays the geodynamic framework of eastern Sicily with major structural domains (modified from Bottari et al., 2020 and Lentini et al., 2006).

3. Data and Metadata Collection

The data used in this study were collected during the geophysical measurement campaigns carried out by different Research Units (Table 1). The dataset includes both new measurements acquired during the geophysical measurement campaigns conducted in 2023, and pre-existing datasets provided by several institutions (i.e., the one from the Sicilia Region, from the Istituto Nazionale di Vulcanologia e di Geofisica, INGV, the University of Catania, UNICT and the Helmholtz Centre for Geosciences, GFZ).

In total, 1,172 HVSR derived from environmental noise measurements were collected. The data were acquired using different types of seismic sensors characterized by cut-off frequencies ranging from 0.2 Hz to 1 Hz. All recordings have a minimum duration of 20 minutes, ensuring adequate signal stability and spectral resolution for reliable HVSR analyses.

Table 1. Overview of the data used in this study. RU is the Research Unit responsible for the dataset.

ID subset	RU	Number of measurements	Type of measurements	Type of instrument and main characteristics	Source
1	CNR IGAG	86	Single station measurements	SARA SL06 Seismograph Recorder (6 channels and 24-bit) + SARA SS02 Velocity Sensor (cut-off frequency at 0.2 Hz)	This study
2	CNR ISPC	132	Single station measurements	EchoTromo HVSR 3	This study
3	GFZ	71	Single station measurements – TOMO ETNA	Broadband-short-period sensors (L4-3D; Trillium)	Ibanez, Jesus M.; Lühr, Birger; Dahm, Torsten (2014): TOMO-ETNA. GFZ Data Services. Other/Seismic Network. doi:10.14470/6G7569676919. https://geofon.gfz-potsdam.de/waveform/archive/network.php?ncode=1T&year=2014
4	INGV	53	Single station measurements	Seismic nodes (Geospace)	This study
5	ISPRA	98	Single station measurements	Tromino	This study
6	OGS	59	Temporary stations and single station measurements	Reftek + Lennartz 1 s + Sentinel Lunitek	This study; ETNA Microzonation Temporary Network, doi:10.7914/gmfh-g622
7	UNICT	212	Single station measurements	Tromino	This study
8	Sicily Region	327	Single station measurements	Tromino	First-level Seismic Microzonation study
9	UNICT – INGV	134	Single station measurements	Tromino	Panzera, F., Lombardo, G., Longo, E., Langer, H., Branca, S., Azzaro, R., ... and Trimarchi, F. (2017). Exploratory seismic site response surveys in a complex geologic area: a case study from Mt. Etna volcano (southern Italy). Natural Hazards, 86 (Suppl 2), 385-399.

The measurements are distributed across thirty-seven municipalities in the province of Catania (Sicily) covering an area of approximately 2,000 km^2 (Fig. 2). Several measurements were acquired in proximity to active fault lineaments, including the Linera-Santa Maria Ammalati (or Santa Tecla-Linera), Fiandaca, and Trecastagni structures.

All relevant metadata including municipality, longitude and latitude, map projection system, elevation value and unit, slope resolution, slope gradient, surficial geology, outcropping engineering-geological technical units (SM working group, 2015), Research unit, RU, sensor type are archived within the associated shapefile and .csv file available in the Zenodo repository (10.5281/zenodo.21300187).

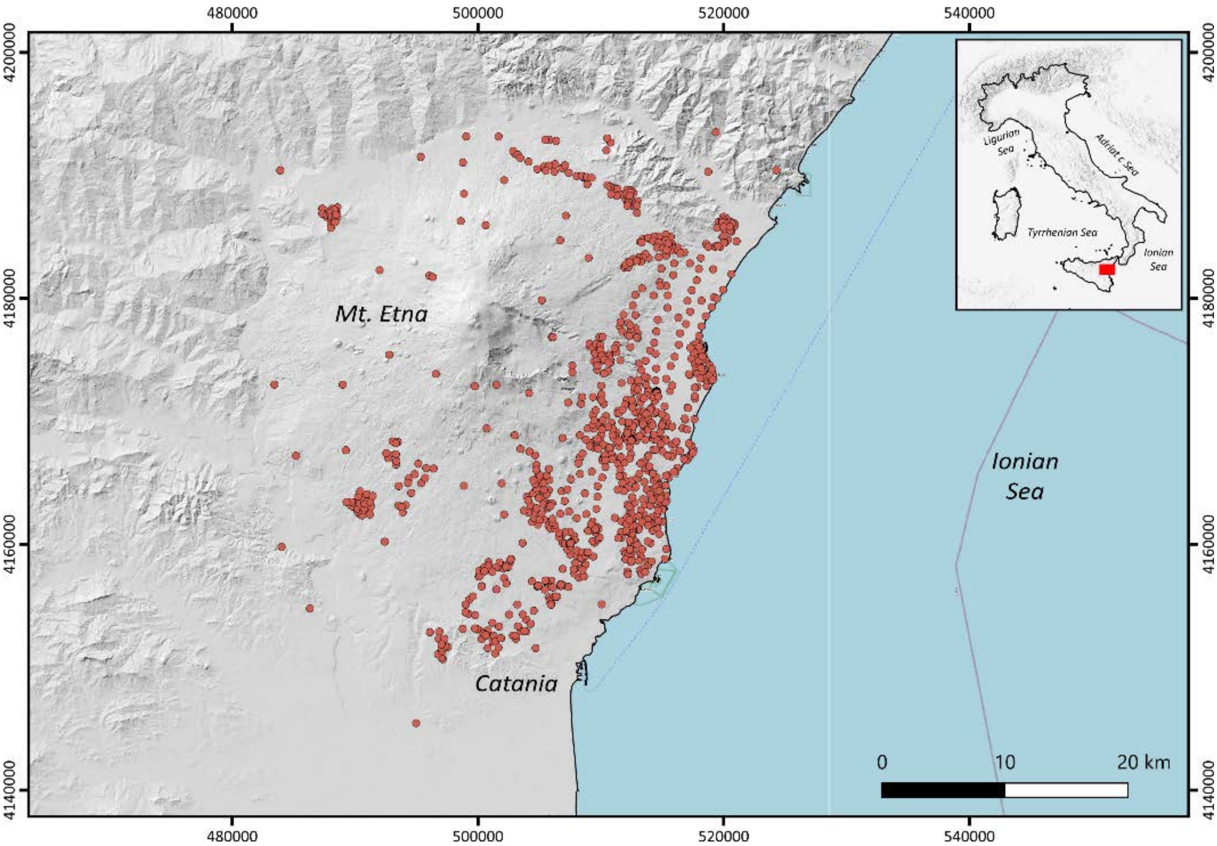

Figure 2. Location of the HVSR measurements.

The number of available HVSR measurements varies across the different municipalities. A sunburst diagram and a histogram (Fig. 3) were produced to illustrate the hierarchical distribution of the dataset, showing both the number of measurements per municipality and the contribution of each research unit or field crew involved in data acquisition. This visualization highlights how the dataset is structured and how data collection efforts have been distributed across the Etnean area.

The highest number of HVSR measurements was collected in the municipalities of Santa Venerina and Acireale. As shown in Fig. 1, which displays the centroids of these municipalities in relation to the location of the main fault systems, most of the HVSR measurements are in proximity of important fault systems. The differentiation among the research units and field crews operating in the area – each of them using different instruments but following standardized acquisition procedures – contributes to the robustness and reliability of the dataset. It is worth underlining that Acireale is the municipality with the highest number of residential buildings according to the ISTAT database (ISTAT, 2021; approximately 10,000 units), which further emphasizes the relevance and potential impact of the dataset.

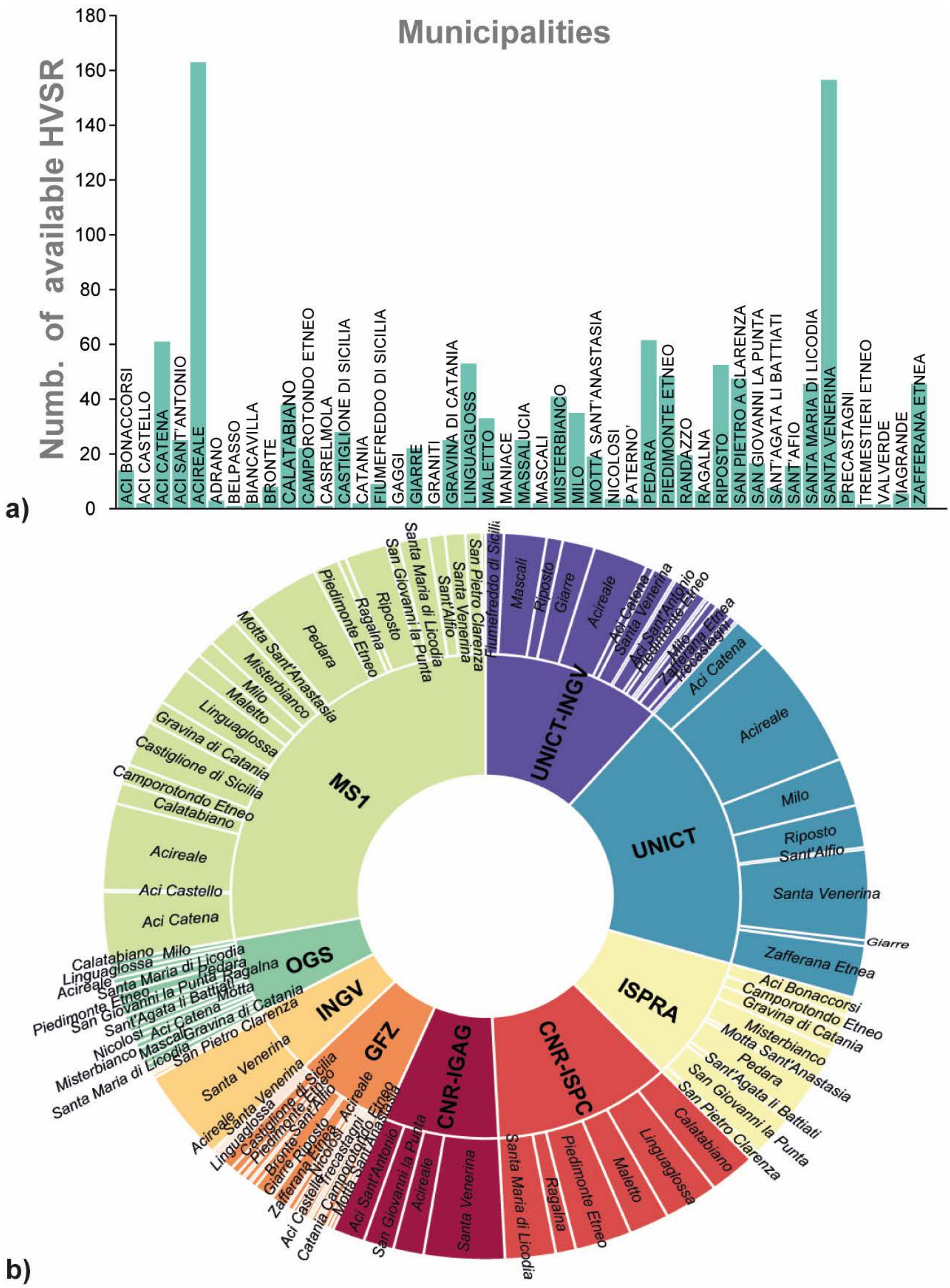

Figure 3. (a) histogram and (b) sunburst of HVSR measurements across municipalities. The sunburst visualization highlights the hierarchical structure of the dataset, showing the number of measurements per municipality and the contribution of each research unit/field crew involved in data acquisition. The Figure was produced using RAWGraphs, an open-source data visualization framework designed for the graphical exploration of structured datasets (https://rawgraphs.io).

3.1 Data manipulation

The basic idea was to construct a unified archive in which all measurements from the nine data subsets are stored as MiniSEED files, the international standard format for storing and transmitting digital seismological time-series data. Each filename corresponding to the unique ID of the measurement.

For subsets 1, 3, 4, and 6, the original data were already available in MiniSEED format. For these subsets, the archive contains one MiniSEED file for each ambient-noise measurement, with no instrumental correction applied. It is straightforward to associate the MiniSEED files with their corresponding measurement locations on the map, as their filenames retain the same root as the original file.

Conversely, the original data of subsets 2, 5, 7, 8, and 9 were acquired in the proprietary .trc format and subsequently reorganized into a new archive of .SAF files, according to the standardized text-based waveform data format developed during the European SESAME Project (Site Effects Assessment Using Ambient Excitations, SESAME Project, 2004). This step required importing .trc files into Grilla, the software specifically developed by the instrument manufacturer for processing Tromino recordings (Moho WG, 2020). The data were then converted into .SAF format to ensure compatibility with the subsequent HVSR processing workflow. Each file contains from 11 to 20 header lines, followed by the noise data in alphanumeric format. Instrumental correction was applied in this case, using Grilla's built-in procedures, which accounts for the following parameters:

- full scale in mV: 5;
- conversion factor from counts to mm/s: 0.00000304469.

The .SAF raw recordings were renamed according to a standardized naming convention (STA_CODE.saf) and stored in the folder named "BACKUP_DATA". Each .SAF file was exported into a single MiniSEED file (one for each noise measurement) using a Python routine executed within a Jupyter Notebook environment, a web-based interactive computational environment which uses open-source libraries. The script performs an automated conversion of all .SAF files contained in the working directory into MiniSEED format. Each .SAF file is assumed to store three-component ambient-noise data (vertical, north-south, and east-west), organized in columns after a fixed header Using ObsPy, an open-source Python framework specifically designed for processing seismological data, data were checked and prepared for the following processing steps: for each file, the three components are loaded and assigned to individual ObsPy Trace objects. These traces are combined into an ObsPy Stream, and any potential gaps or overlaps are merged. Finally, one MiniSEED file is written per station, using the station code as the output filename.

It is then straightforward to associate the MiniSEED files with their corresponding measurement locations on the map, as their filenames retain the same root as the original .SAF file.

Since measurements were acquired using different sampling frequency rates (see metadata file in the Zenodo folder), depending on the characteristics of the digitizers, before applying the instrumental correction to the raw recordings of subsets 2, 5, 7, 8, and 9, all traces were resampled to 128 sps if necessary.

All the MiniSEED files are stored in the folder named "RAW_DATA".

3.2 HVSR analyses

The HVSR curves were computed from ambient noise recordings using the open-source Python package HVSRpy (v. 2.1.0, Cox et al., 2020; Cheng et al., 2020; Vantassel, 2020, 2024), a recently developed tool for HVSR analysis. The processing workflow follows established best practices and is consistent with the recommendations of the SESAME Project (2004). A linear detrend was applied to each time series, which was then segmented into 60 s windows. A band pass filter between 0.2 and 20 Hz was used to retain the frequency range relevant for site response analysis. Sensor orientation was kept fixed at 0° from North, and windows with non-uniform sampling intervals were retained for subsequent correction during frequency domain processing.

HVSR curves were computed using the standard method implemented in HVSRpy (v. 2.1.0). Each window was tapered with a Tukey window ($\alpha = 0.1$), corresponding to a 5% cosine taper at both ends of the time series. Spectral smoothing was performed using the Konno-Ohmachi (1998) operator with a bandwidth parameter of 40, evaluated over 200 logarithmically spaced frequencies between 0.2 and 20 Hz. The two horizontal components were combined using the geometric mean, and windows with dissimilar time steps were corrected using frequency domain resampling.

To improve the robustness of results, we applied the frequency domain window rejection algorithm proposed by Cox et al. (2020). This procedure evaluates each 60 s window in the frequency domain and identifies those whose spectral shape deviates significantly from the ensemble of all windows. The rejection criterion was defined using n = 2 standard deviations within the frequency band 0.2-20 Hz, corresponding to the range of engineering interest for shallow site response (see Fig. 4). This filtering step ensures a statistically consistent dataset and reduces the influence of outliers or transient noise contamination.

For each window, individual HVSR curves are calculated and then combined under the assumption of a log-normal distribution. This approach enables estimation of a mean HVSR curve along with its associated variability, expressed as a one standard deviation envelope.

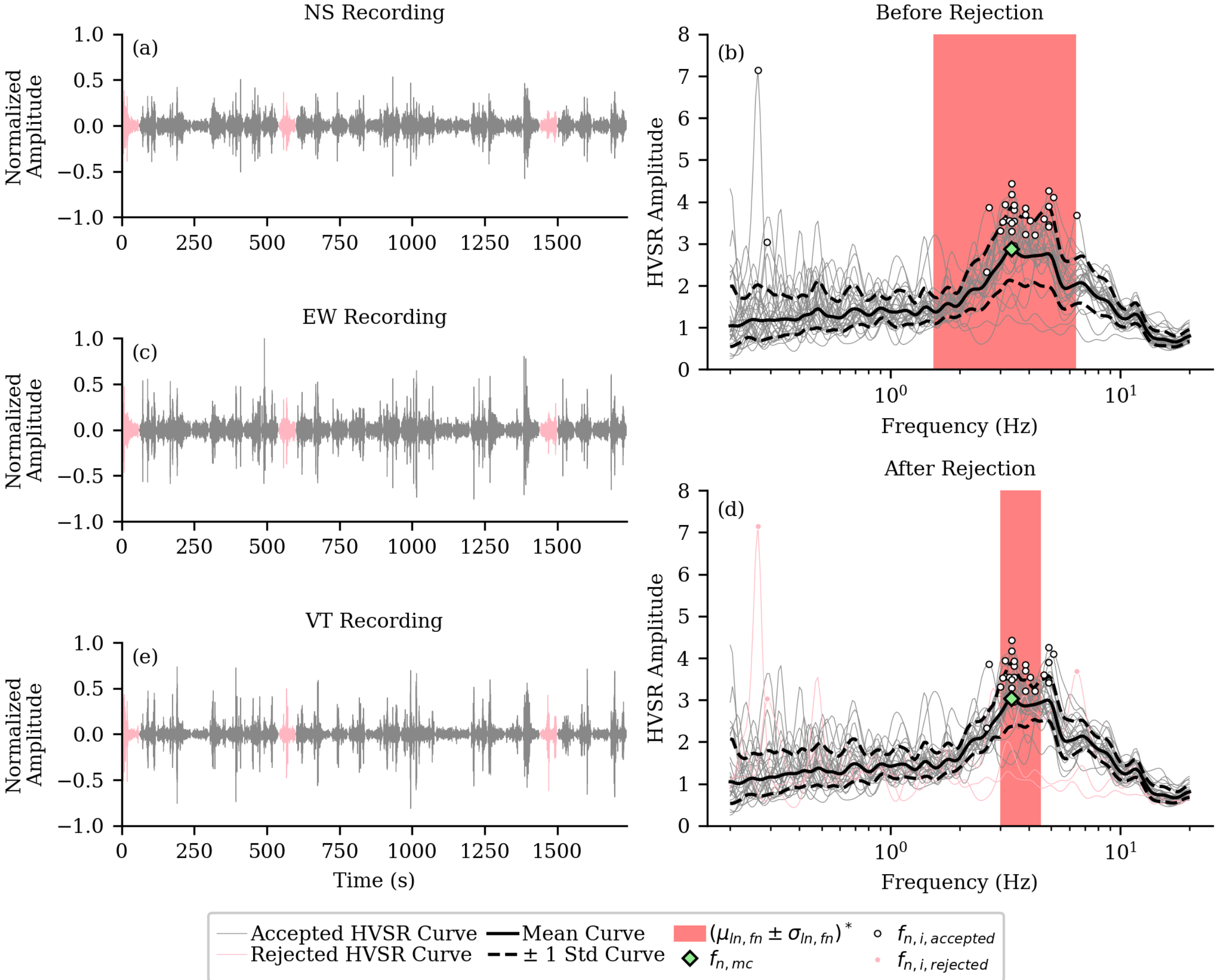

Figure 4. Example output of the HVSR curve at station A32. Accepted and rejected single-window HVSR curves are shown together with the mean curve and its ±1 standard deviation envelope. The shaded red band highlights the frequency range corresponding to the fundamental resonance peak.

The outcomes of the HVSR analysis are shown in Fig. 5 and grouped by municipality for clarity. The shapes of the HVSR curves are widely scattered across the analysed frequency range (0.2-20 Hz). Since the shape of HVSR curves reflects resonance phenomena potentially associated with seismic impedance contrasts – key elements for the seismic characterization of the subsurface – the substantial variability observed in Fig. 5 provides a qualitative indication of the marked heterogeneity of the subsoil.

To assess the internal consistency of the dataset, we compared HVSR curves obtained from closely spaced measurements (maximum 436 m) and acquired with different instruments. Figure 6 shows the comparison between six HVSR curves collected during the TOMO-ETNA campaign (dataset 3 in Table 1), an equal number of measurements acquired during the first-level Seismic Microzonation survey (dataset 8 in Table 1) and one acquired by

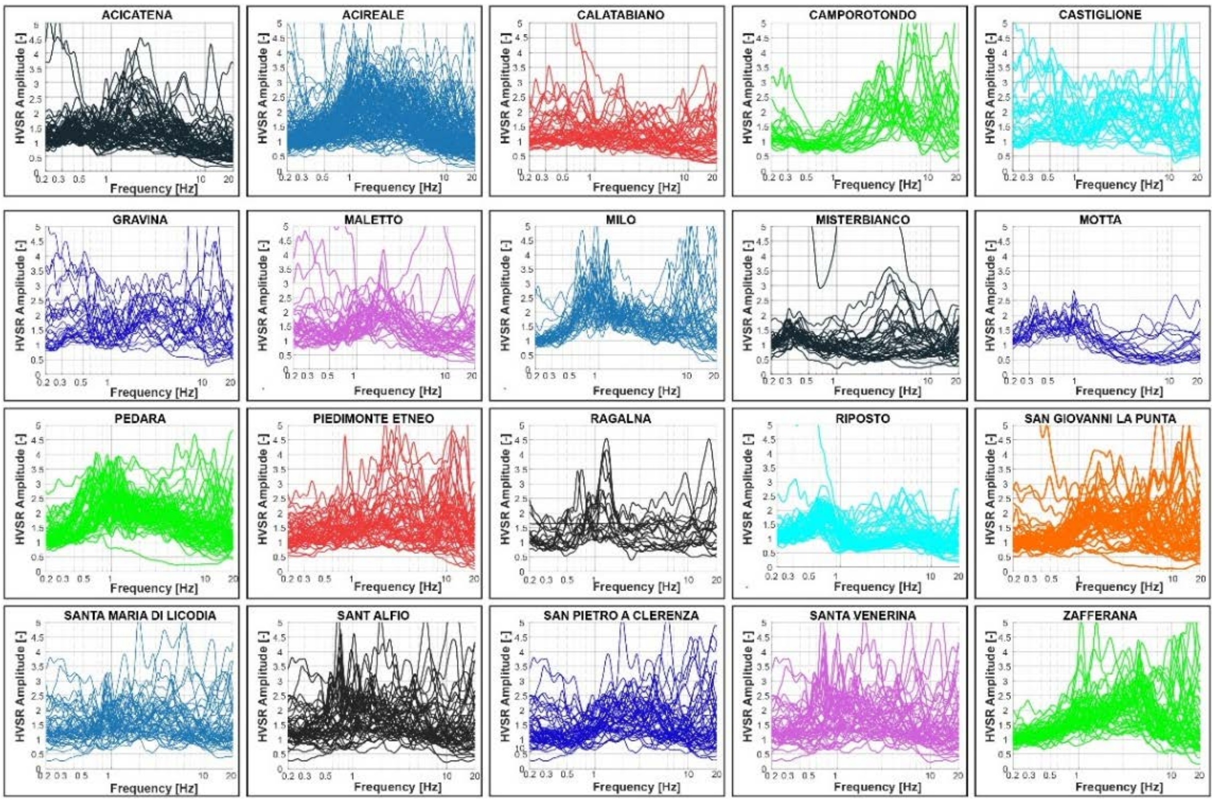

Figure 5. Summary of the HVSR measured grouped for municipality.

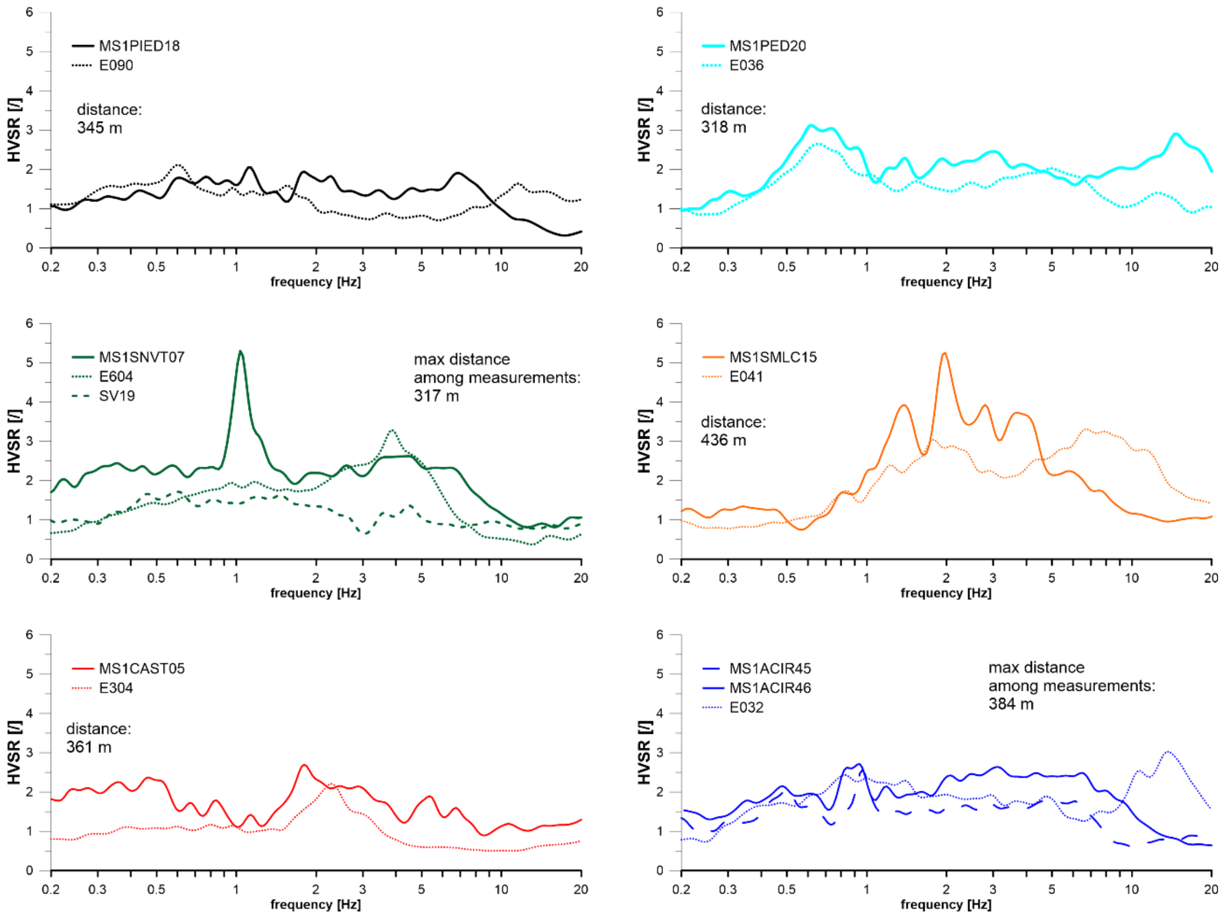

Figure 6. Comparison between HVSR obtained at closely spaced measurements acquired with different sensors.

UNICT (dataset 7 in Table 1). The results show a good agreement between the measurements obtained with the different instruments, except measurements MS1SNVT07 which shows lower consistency with the other available. The SV19 curve exhibits a shape typical of an anthropic peak. It has to be highlighted that the purpose of performing these comparisons is to verify the reliability of the measurements integrated into the dataset, which were acquired at different times, with different sensors whose instrumental response has not been validated before acquisitions. Since the study area is a geological volcanic setting, a high lateral variability is expected, as the shallow layers may have different thicknesses and physical properties. Conversely, at low frequencies the geological structure is less variable, and therefore the same frequencies can be detected even at distances shorter than 350 m. By fixing 1 Hz as the reference frequency and considering minimum shear wave velocities of 350 m/s, we obtain a propagation wavelength of approximately 350 m that justifies the choice of adopting a radius of 350 m for this consistency check. Higher shear-wave velocities may correspond to even longer wavelengths.

3.3 Example of data usage: Peak identification analysis

The predominant resonance frequency (*fd*) is identified as the frequency corresponding to the maximum amplitude of the mean HVSR curve. In addition to providing the mean HVSR curve and its variability (±1 standard deviation), estimated assuming a log-normal distribution from individual HVSR curves computed over 60 s windows, HVSRpy also derives statistical information on the peak frequencies of the single-window curves. This approach ensures a more robust statistical representation and helps reduce ambiguity in the selection of the predominant frequency (*fd*), whether derived from the mean HVSR curve or from the distribution of individual window peaks. The HVSRpy traces both sets of amplitude values: the amplitude at the predominant frequency identified on the mean curve, and the amplitudes associated with each window.

Moreover, as stated by Cox et al. (2020), adopting a log-normal distribution for *fd* ensures statistical interchangeability between *fd* and its reciprocal, the predominant site period (T0). This property is particularly relevant in the present case study, since T0 plays a crucial role in ground-response analyses and represents a key parameter in several existing and proposed seismic site-classification schemes. (Standards New Zealand 1170.5, 2004; Pergalani et al., 2019). Furthermore, experimental observations indicate that, for stable and reliable measurements, the mean of the individual peak frequencies closely approximates the peak of the mean HVSR curve (see Fig. 7). As a result, the method mitigates ambiguity in selecting the representative *fd* value, whether derived from the mean HVSR curve or from the statistical distribution of individual peak frequencies.

Statistical analyses of peak frequency confirm the need to consider both peak-value estimation and its associated uncertainties. The interpretation of the distributions derived from the individual HVSR windows shows a shift of the first resonance peak toward slightly lower frequencies (from approximately 2 Hz to about 1 Hz, Fig. 7a). As shown in Fig. 2, large part of the HVSR measurements is set in the lower part of Mt. Etna, where deeper soils are expected to be present. This is confirmed in Fig. 5, where the HVSR curves belonging to Castiglione, Motta and Gravina municipalities, have higher amplification at lower frequencies, below 1 Hz (Fig. 7c). On the other hand, the analysis of the mean HVSR curve reveals a splitting of the main peak between 1 and 3 Hz (Fig. 7d vs Fig. 7c). The maximum peak amplitudes and mean-curve peak amplitudes lie in the ranges 2-4 and 2-3, respectively (Fig. 7e and f). The amplitude peaks below 2 in Fig. 7e and 7f are not consistent with the SESAME Project (2004) guidelines, according to which only peaks with amplitudes clearly exceeding 2 can be regarded as meaningful. In this analysis, all peaks were retained to ensure an unbiased processing of the data. Considering that resonance values in the 2-10 Hz range are particularly relevant for typical one- to four-storey residential buildings (Pergalani et al., 2019), the analysis of resonance frequencies becomes essential for defining appropriate seismic-risk mitigation strategies, even though the median amplitude values remain moderate.

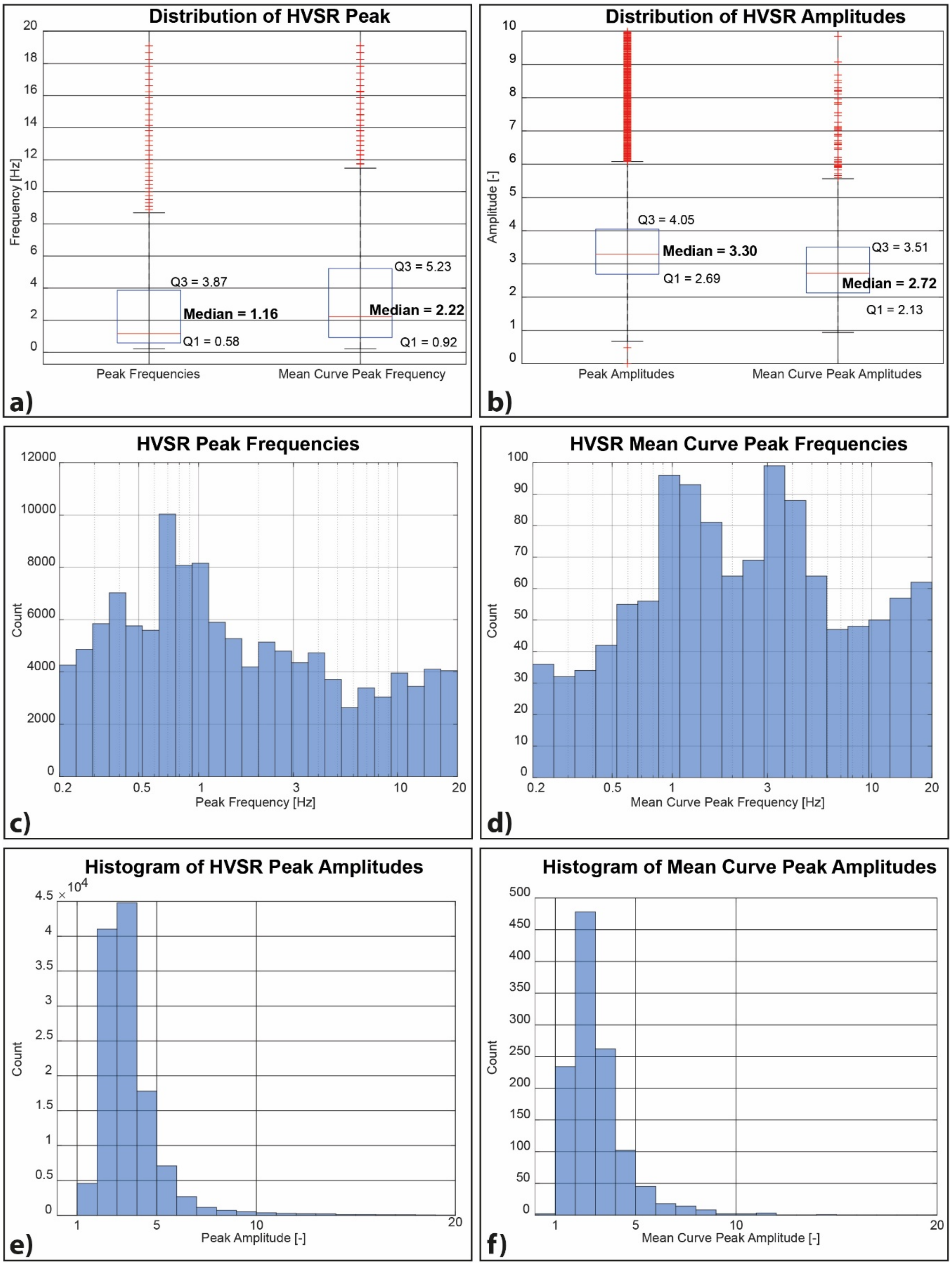

Figure 7. (a) distribution of HVSR peak frequencies and mean-curve peak frequencies fd through comparative boxplots; (b) comparative boxplots of peak and mean-curve peak amplitudes Ad; (c) logarithmic histogram of all peak frequencies; (d) logarithmic histogram of mean-curve peak frequencies fd; (e) distribution of all HVSR peak amplitudes; (f) distribution of mean-curve peak amplitudes Ad. In (a) and (b), on each box, the central line represents the median, while the lower and upper edges correspond to the 25^{th} and 75^{th} percentiles, respectively. The whiskers extend to the most extreme data points that are not classified as outliers, whereas outliers are displayed individually using the '+' marker.

3.4 Jupyter Notebook

The dataset presented combines heterogeneous source files: a georeferenced shapefile of measurement sites, a tabular summary of HVSR analysis results, individual HVSR curve files, and raw seismic records in MiniSEED format. To support the development of an analytical and visualization workflow, three Jupyter notebooks were created.

The first notebook consolidates the raw data into a single, self-contained GeoPackage (.gpkg) database. This format, adhering to the internationally recognized standards set by the Open Geospatial Consortium (OGC, https://www.ogc.org/standards/), is open and ensures direct interoperability with GIS software such as QGIS and with Python geospatial libraries, while preserving all relational links between site metadata, derived parameters, and raw data (Fig. 8). The geodatabase is built by joining the geographic and tabular data through a common site identifier and by embedding relative file paths to the associated raw data, producing a GeoPackage that serves as the single source of truth for all subsequent analyses.

The second notebook provides an interactive exploratory environment, including descriptive statistics, frequency and amplitude distributions, correlation scatter plots, an interactive map, and a dynamic HVSR curve viewer. This viewer allows users to filter sites by parameter ranges, overlay and compare multiple spectral curves with optional standard-deviation bands, and export filtered subsets to the most common output formats (e.g., CSV or GeoJSON).

The third notebook delivers a deployable Panel web dashboard (Fig. 9) that consolidates the key functionality, namely interactive site filtering, HVSR curve visualization, and direct download of the HVSR and MiniSEED files for any selected site, into a standalone application that can be served without dedicated server infrastructure.

The notebooks are available in a GitHub repository (https://github.com/fpennica/hvsr-db). The entire environment is fully specified through a Conda environment file, a specific software which manages both the Python files as well as packages from multiple programming languages and can be launched on any operating system using the provided shell scripts, or executed in the cloud with no local installation required (e.g. through Binder, a tool that allows to turn a code repository into an interactive, shareable computing environment via a web browser).

This design prioritizes reproducibility and accessibility, allowing researchers to explore the data and adapt the workflow to comparable datasets, thereby supporting data sharing and collaborative use. In fact, updated or newly acquired data can be added to the data directory, provided that the original folder and file structure is preserved. Once the data are inserted, the visualisation of the measurements is automatically refreshed.

site
site_ID
name
municipality
longitude
latitude
mapProjectionSystem
elevation_value
elevation_unit
slopeResolution
slopeGradient
terrainClass
surficialGeology
surficialUGT
field_crew
sensor
raw_Data_link

hvProcessing
hvProcessing_ID
hv_Data_ID
site_ID
mean_removal
time_window_length
window_overlap
taper_type
taper_width
number_windows
anti_trigger
bad_sample_tolerance
bad_sample_threshold
deltaT_STA
deltaT_LTA
min_STA_LTA
max_STA_LTA
high_pass_filter
high_pass_corner_frequency
high_pass_filter_type
smoothing_type
smoothing_constant
horizontal_combination
distribution
comments
hv_Data_link

fd_Ad_and_LD_frequencies
fundamental_frequency_ID
hvProcessing_ID
f0
A0
fd
Ad

HVSR_csv
hv_Data_ID
fundamental_frequency_ID
hv_Data_link

BACKUP_DATA
backup_Data_ID
fundamental_frequency_ID
raw_Data_link

Figure 8. Tables, fields, and primary (gold) and foreign (orange) keys in HVSR database schema.

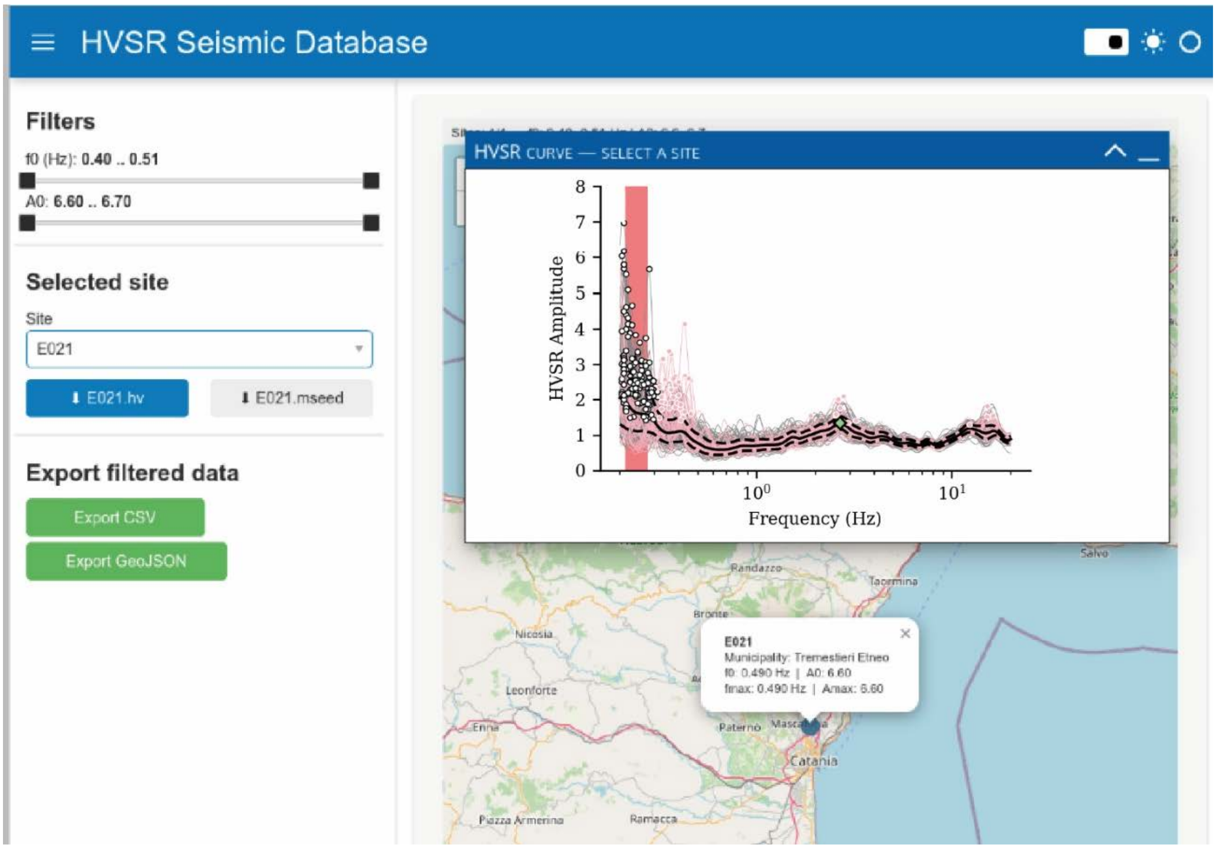

Figure 9. Example usage of the HVSR data.

4. Conclusions

Recovering the information collected during this study and previous ones can be extremely valuable for obtaining a preliminary overview of the predominant frequencies within the study area.

The archive is intended to facilitate the standardization of data required for Seismic Microzonation studies. In terms of potential applications, it can support the calibration of seismic stratigraphies used in numerical modelling for assessing local seismic response, as well as their integration with available estimates of building resonance periods. It is worth noticing that this archive may be very useful for further investigating the role of lateral heterogeneity and structural complexity in modulating HVSR propagation in volcanic terrains.

The dataset also proves to be highly valuable for the analysis of rotational HVSR. Indeed, considering that within the framework of the ETNA FAC MS project a new fault database has been developed to support the reclassification of tectonic structures according to the criteria defined in the third level Seismic Microzonation guidelines (MS3), this HVSR archive can contribute to further investigations on polarization along faults and to the testing and developing of methodologies for the preliminary identification of fault indicators.

Possible limitations may arise when the automatic picking of f_0 is used without appropriate cautionary criteria. The estimated f_0 may include significant and stable peaks generated by monochromatic disturbances associated with industrial plants or engines. No detection strategy has been implemented to remove these disturbances. The same applies to the automatic removal of transients: when the ambient vibration wavefield is weak, transients may provide useful signal information. Moreover, the variability in resolution and accuracy among the instruments used must be considered (Fig. 6 is an illustrative example).

The overall intention is to provide a reproducible model for conducting research and developing workflows in the field of seismic microzonation and related disciplines. The Jupyter Notebook routines are designed to be used whenever new measurements become available, including those collected outside the studied area. Based on this experience, we strongly encourage the homogenization, archiving and sharing of HVSR data – and geophysical datasets in general. This procedure ensures the reproducibility of results and enables further refinement and enhancement of analyses.

Data availability statement. Data can be downloaded at: https://zenodo.org/uploads/21300187.

Acknowledgements. The authors acknowledge the professionals and technicians who contributed to the field campaigns and data acquisition. We sincerely thank the Editor and the Reviewers for their thoughtful and constructive comments, which have greatly contributed to improving the quality and clarity of the manuscript. We are particularly grateful to Anna Grazia Chiodetti for her invaluable support throughout the editing and typesetting process.

References

Azzaro, R. (1999). Earthquake surface faulting at Mount Etna volcano (Sicily) and implications for active tectonics. J. Geodyn., 28, 2, 193-213.

Azzaro, R., S. Branca, K. Gwinner and M. Coltelli (2012). The volcano-tectonic map of Etna volcano, 1:100,000 scale: an integrated approach based on a morphotectonic analysis from high-resolution DEM constrained by geologic, active faulting and seismicity data, Ita. J. Geosci., 131(1), 153-170.

Bottari, C., S. Giammanco, D. Cavallaro, F. Sortino et al. (2020). How to reveal unknown hidden faults and historical earthquake damage applying multidisciplinary methods in archaeological sites: The case of mid-third century CE Mt. Etna earthquake (Eastern Sicily, Italy). Tectonophysics, 790, 228544, doi:10.1016/j.tecto.2020.228544.

Cara, F., G. Cultrera, G. Riccio, S. Amoroso et al. (2019). Temporary dense seismic network during the 2016 Central Italy seismic emergency for microzonation studies, Sci. Data, 6, 182, doi:10.1038/s41597-019-0188-1.

Catalano, S., A. Bonforte, F. Guglielmino, G. Romagnoli et al. (2013). The influence of erosional processes on the visibility of Permanent Scatterers Features from SAR remote sensing on Mount Etna (E Sicily), Geomorphology, 198, 128-137, doi:10.1016/j.geomorph.2013.05.020.

Cheng, T., B. R. Cox, J. P. Vantassel and L. Manuel (2020). A statistical approach to account for azimuthal variability in single-station HVSR measurements, Geophys. J. Int., 223, 2, 1040-1053. ISSN: 0956-540X, doi:10.1093/gji/ggaa342.

Cox, B. and J. Vantassel (2018). Dynamic Characterization of Wellington, New Zealand, Design Safe-CI. https://www.designsafe-ci.org/data/browser/public/designsafe.storage.published/PRJ-2075.

Cox, B. R, T. Cheng, J. P. Vantassel and M. Lance (2020). A statistical representation and frequency-domain window-rejection algorithm for single-station HVSR measurements. Geophysical Journal International 221.3, pp. 2170-2183. ISSN: 0956-540X, eprint: https://academic.oup.com/gji/article-pdf/221/3/2170/33173960/ggaa119.pdf, doi:10.1093/gji/ggaa119.

Cultrera, G., P. Bordoni, A. Mercuri, M. Quintiliani et al. (2022). Database for site characterization of permanent seismic stations (CRISP). Istituto Nazionale di Geofisica e Vulcanologia (INGV), doi:10.13127/crisp.

D'Amico, V., M. Picozzi, F. Baliva et al. (2008). Ambient noise measurements for preliminary site-effects characterization in the urban area of Florence, Italy, Bull. Seismol. Soc. Am., 98, 3, 1373-1388, doi:10.1785/0120070231.

Di Giulio, G., F. Cara, A. Rovelli, G. Lombardo and R. Rigano (2009). Evidences for strong directional resonances in intensely deformed zones of the Pernicana fault, Mount Etna, Italy, J. Geophys, Res.: Solid Earth, 114, B10308.

Gallipoli, M. R., M. Mucciarelli, A. Masi, P. Harabaglia et al. (2004). Analysis of RC building dynamic response and soil-building resonance based on data recorded during a damaging earthquake (Molise, Italy, 2002), Bull. Seismol. Soc. Am., 94, 5, 1943-1953.

Gospe, T, P. Wang, P. Zimmaro and J. P. Stewart (2020). HVSR database and multi-measurement consistency for California sites, Proc. SMIP2020 Seminar on Utilization of Strong Motion Data, California Strong Motion Instrumentation Program, Web Conference, Retrieved from https://escholarship.org/uc/item/9165t893.

Hobiger, M., P. Bergamo, W. Imperatori, F. Panzera et al. (2021). Site Characterization of Swiss Strong-Motion Stations: The Benefit of Advanced Processing Algorithms, Bull. Seismol. Soc. Am., doi:10.1785/0120200316.

Imposa, S., G. Coco and M. Corrao (2004) "Site effects close to structural lineaments in eastern Sicily (Italy), Engin. Geol. 72, 3-4, 331-341.

Imposa, S., F. Panzera, S. Grassi, G. Lombardo et al. (2017). Geophysical and geologic surveys of the areas struck by the August 26th 2016 Central Italy earthquake: the study case of Pretare and Piedilama, J. Appl. Geophys., 145, 17-27.

ISTAT (2021). Censimento permanente della popolazione e delle abitazioni – Edifici e unità immobiliari. Last accessed: [25.04.2026]. https://www.istat.it/it/archivio/104317.

Konno, K. and T. Ohmachi (1998). Ground-motion characteristics estimated from spectral ratio between horizontal and vertical components of microtremor, Bull. Seismol. Soc. Am., 88, 1, 228-241, doi:10.1785/BSSA0880010228.

Laurenzano, G. et al. (2026). Empirical amplification factors for seismic microzonation studies in volcanic regions: the study case of Mt. Etna (Italy). Submitted to this issue.

Lentini, F., S. Carbone and P. Guarnieri (2006). Collisional and postcollisional tectonics of the Apenninic-Maghrebian orogen (southern Italy). In: Special Paper Geol. Soc. Am., 409, 57-81, doi:10.1130/2006.2409(04).

Mascandola, C., M. Massa, S. Barani et al. (2019). Mapping the seismic bedrock of the Po Plain (Italy) through Ambient-Vibration Monitoring, Bull. Seismol. Soc. Am. 109, 1, 164-177, doi:10.1785/0120180193.

Moscatelli, M., D. Albarello, G. Scarascia Mugnozza and M. Dolce (2020) The Italian approach to seismic microzonation, Bull. Earthqu. Engin., 18, 5424-5440. doi:10.1007/s10518-020-00856-6.

Moho, W. G. (2020). Tromino International patents: Pub. No. WO2006011021 (A1), Pri. No. IT2004BO00449 20040719, USPTO 7.800.981. User's manual. Disponibile online, previo accesso all'area riservata, all'indirizzo: https://moho.world/tromino/ (ultimo accesso: 22.05.2023).

Panzera, F., G. Lombardo and C. Monaco (2016). New evidence of wavefield polarization on fault zone in the lower NE slope of Mt. Etna, It. J. Geosci., 135, 2, 250-260.

Panzera, F., G. Lombardo, E. Longo, H. Langer et al. (2017). Exploratory seismic site response surveys in a complex geologic area: A case study from Mt. Etna volcano (southern Italy), Nat. Hazards, 86, 2, 385-399.

Panzera, F., G. Tortorici, G. Romagnoli, G. Marletta and S. Catalano (2020). Empirical evidence of orthogonal relationship between directional site effects and fracture azimuths in an active fault zone: The case of the Mt. Etna lower eastern flank, Engin. Geol., 279, 105900.

Parolai, S., P. Bormann and C. Milkereit (2002). New relationships between Vs, thickness of sediments, and resonance frequency calculated by the H/V ratio of seismic noise for the Cologne area (Germany), Bull. Seismol. Soc. Am., 92, 6, 2521-2527, doi:10.1785/0120010248.

Pergalani, F., A. Pagliaroli, C. Bourdeau, M. Compagnoni et al. (2019). Seismic microzoning map: approaches, results and applications after the 2016-2017 Central Italy seismic sequence, Bull. Earthqu. Engin., 18, 5595-5629.

Peronace, E., R. Azzaro, S. Catalano, M. Mancini and A. Torrisi (2026). The "Etna FAC-MS3" Project: Problems and implications of capable faults on microzonation in a Volcanic area, GNGTS 2026, Abstract Books, 1, 1, 133-137.

Pischiutta, M., A. Rovelli, F. Salvini, G. Di Giulio and Y. Ben-Zion (2013). Directional resonance variations across the Pernicana fault, Mt. Etna, in relation to brittle deformation fields, Geophys. J. Int., 193, 2, 986-996, doi:10.1093/gji/ggt031.

Porchia, A., G. Tortorici, A. D'Agostino, E. Peronace et al. (2026). A GIS based Approach for Planning Investigations in Seismic Microzonation Studies of Level 3: Methodology and Application in the Etnean Area, Italy. Ann. Geophys. 2026, 69, doi:10.4401/ag-9532.

Rigano, R., F. Cara, G. Lombardo and A. Rovelli (2008). Evidence for ground motion polarization on fault zones of Mount Etna volcano, J. Geophys. Res.: Solid Earth, 113, B10, doi:10.1029/2007JB005574.

SESAME Project (2004). Guidelines for the implementation of the H/V spectral ratio technique on ambient vibrations measurements, processing and interpretation, SESAME European research project EVG1-CT-2000-00026.

SM working group (2015). Guidelines for Seismic Microzonation. Conference of Regions and Autonomous Provinces of Italy – Civil Protection Department, Rome, 124.

Standards New Zealand (SNZ) (2004). Structural Design Actions – Part 5 Earthquake Actions – New Zealand, NZS 1170.5:2004, Wellington, New Zealand.

Technical Commission on Seismic Microzonation (2015) Land Use Guidelines for Areas with Active and Capable Faults (ACF), version 1.0. Conference of the Italian Regions and Autonomous Provinces – Civil Protection Department, Rome, 66, https://centromicrozonazionesismica.it/it/strumenti/linee-guida-ms/.

Vantassel, J. P. (2020). hvsrpy: latest (Concept). Zenodo. doi:10.5281/zenodo.3666956.

Vantassel, J. P. (2025). hvsrpy: An Open-Source Python Package for Microtremor and Earthquake Horizontal-to-Vertical Spectral Ratio Processing, Seismol. Res. Lett., 96, 4, 2671-2682, doi:10.1785/0220240395.

Wang, P, P. Zimmaro, T. E. Buckreis, T. Gospe et al. (2022). Relational database for Horizontal-to-Vertical Spectral Ratios, Seism. Res. Lett., 93, 2A, 1075-1088.

Wang, P., P. Zimmaro, S. K. Ahdi, A. Yong and J. P. Stewart (2023). Identification protocols for horizontal-to-vertical spectral ratio peaks, Bull. Seismol. Soc. Am., 113, 2, 782-803.

***CORRESPONDING AUTHOR:** **Carla BARNABA**,
Istituto Nazionale di Oceanografia e di Geofisica Sperimentale, Italy
e-mail: cbarnaba@ogs.it